energies

MDPI

Article

Analysis of Selected Operating States of the Line Start Synchronous Reluctance Motor Using the Finite Element Method

Paweł Idziak * and Krzysztof Kowalski

Division of Mechatronics and Electrical Machines, Institute of Electrical Engineering and Electronics, Poznan University of Technology, ul. Piotrowo 3a, 60-965 Poznan, Poland; krzysztof.kowalski@put.poznan.pl
* Correspondence: pawel.idziak@put.poznan.pl

Abstract: The article presents the results of work on an effective numerical study of selected transient states of a low-power electrical machine. The object of detailed research was a synchronized squirrel-cage induction motor. Its ability to work at a synchronous speed was enabled by obtaining reluctance torque, caused by an imposed asymmetry between the direct and quadrature reluctances of the rotor. The difference between the reluctances was achieved by changing the rotor geometry by milling additional deep grooves. The modifications of the rotor did not damage the continuity of the rotor cage. Imposed lots were arranged symmetrically around the rotor circumference. In order to study the performance of the modified motor, a parameterized, numerical model of the machine was developed to evaluate the impact of the geometry of the slots. The developed three dimensional (3D) model of the electromagnetic phenomena in the studied magnetic circuit employs the finite element method (FEM). The model takes into account the saturation of the machine's magnetic circuit and the skew of the rotor cage bars as well as the mechanical equilibrium of the terrain system including the moment of inertia and frictional torque in the bearings as well as the load torque resulting from the operation of the internal fan. The simulation study concerned the starting process of the machine under different values of the load. The influence of the supply voltage phase angle at the moment of start-up and the initial position of the rotor in relation to the stator was investigated. In order to calibrate the model, tests of the physical object were performed. The corrections introduced concerned the magnetization characteristics of the magnetic circuit. The results obtained confirm the correctness of the adopted strategy of testing the operational properties of the considered engine.

Keywords: reluctance motor; finite element analysis; three-dimensional field model; electromagnetic torque

Citation: Idziak, P.; Kowalski, K. Analysis of Selected Operating States of the Line Start Synchronous Reluctance Motor Using the Finite Element Method. *Energies* **2021**, *14*, 6825. https://doi.org/10.3390/en14206825

Academic Editors: Lorand Szabo, Anouar Belahcen and Adolfo Dannier

Received: 13 April 2021
Accepted: 11 October 2021
Published: 19 October 2021

1. Introduction

The ever-increasing cost of electricity is pushing users to look for devices that are as efficient as possible. This parameter has become one of the leading criteria for evaluating a device. This applies equally to drives, heating devices, or control and energy distribution systems. In the case of electric drives, all of their components—the motor or electrical to mechanical energy converter (linear motor, inductor, actuator, etc.), the control and power supply system of the converter as well as the regulation and control components—are subjected to independent assessment. In a correctly designed and implemented drive system, the greatest energy losses will usually occur in the electrical to mechanical energy converter itself and mechanical gearboxes if applied. The opposite is true when it comes to the problem of operational reliability. It is intuitively assumed that the more complex the drive system is, the more components it contains and the lower the operational reliability of the system. This belief is confirmed by studies on the reliability of systems containing electronic and electromechanical components [1–5]. Modern electromechanical and electromagnetic transducers themselves are highly reliable components. In many industrial applications,

the electromechanical transducers with the ability to start-up by direct connection to the grid provide a more reliable solution when variable speed operation is not required.

The subject undertaken by the authors takes on significant meaning in view of the commonly accepted trend of minimizing the costs of producing goods. In the case of the electric drive, the costs of production, operation, and exploitation of engines, are equally important. The production costs are partially minimized by limiting the number of mutations of individual components—in the case of the electric motor (e.g., by using the same structure of the stator and its windings). The costs of the process, leading to a satisfactory final solution, can be reduced by using digital (numerical) prototyping. The main disadvantage of this approach is the still existing inability to consider the influence of mechanical technology and thermal processing of details on the final parameters of the manufactured machine. However, such prototyping allows one to limit the number of physical models of the built device. The article shows the effects of using one possible methods such as digital prototyping based on "calibrating" the numerical model through corrections defined for selected manufacturing technologies and determined by a physical experiment. It has been shown that this approach allows for a good determination of the selected functional properties of the machine. A line start reluctance motor (LSRM) was selected as the main research object. In the described case, the behavior of the machine in a transitional state was presented. In the process of modeling and simulating the machine start-up, the following were taken into account: saturation of the magnetic circuit fragments and equations of motion were introduced. The numerical model also takes into account the connection configuration of the stator windings. In the presented experiment, the voltage forcing was used, in other words, the one that occurs in the conditions of the actual machine operation (power supply with full voltage of the network). The entire problem was considered in three-dimensional space. In the descriptions found in the literature, no information has been found on such a broad treatment of the start-up of the LSRM. The results of the calculations were compared with the results of the tests of the physical motor model. Particular attention has been paid to the influence of rotor geometry on the motor's ability to synchro. The aim was to demonstrate the thesis that modern numerical tools, supported by a well-planned physical experiment, allow for the correct analysis of transient states of electrical machines.

The subject of this paper was the design and analysis of a direct-starting, low-power, synchronous reluctance motor. The studied machine is planned to be used as an auxiliary drive element of a larger industrial installation (e.g., a ventilation system). The presented model was developed as a modification of a Sg71-6B type, mass produced, general purpose, squirrel-cage induction motor with a power of 250 W and a synchronous rotational speed of 1000 rpm. Similar approaches to the problem of the development of drives operating at synchronous speeds can be found in the scientific literature as well as in the proposed commercial solutions [6,7]. One of the most important criteria for the correctness of the design procedure is the maximization of the efficiency of the motor for selected load conditions [8,9].

In the presented studies, it was assumed that:

The modified motor should be capable of starting without the use of any additional systems or special starting procedures, at an external load torque of no less than 40% of the rated torque of the induction motor;

The motor, when loaded with the above-mentioned static torque, should fall into synchronism; and

Each time the motor is overloaded, it should pass into an asynchronous operation mode and its unloading should result in the return to a synchronous operation mode.

In the considerations, the use of switched reluctance motors for the design was intentionally rejected. The running capacity of such structures is interesting indeed, but the necessity of additional control and regulation equipment makes such a hybrid drive system more susceptible to failures and thus less reliable [6,7,10,11].

The high reliability of the drive system is especially important when access to the drive components is very difficult (for drives that are built into the installation). The structure considered in this article should be correctly defined as a synchronized squirrel-cage induction motor.

The results of the experiments presented in the latter part of this paper concern both the tests carried out with the physical object before and after the introduction of the modifications as well as the results of the simulation studies using the proprietary numerical model of the tested motor employing the 3D FEM.

The proposed approach reduces the costs of making physical models of the machine, but increases the costs related to the computation time. It has been shown that the synergy of numerical research and physical experiments should be a trend in the modern methodology of electrical machinery production.

2. Structure of the Studied Induction Motor and Its Modifications

A size 71, six-pole asynchronous motor with a squirrel-cage rotor was used in the tests. The rated power of the motor was 250 W and its rated torque of 2.6 Nm at 905 rpm. The motor has an IP rating of 44 (IP—Ingress Protection in accordance with the European Standard EN 60529:2). The rotor cage is die-cast in A2 grade aluminum (according to the information received from the manufacturer). The motor shaft is supported by rolling bearings of the basic series. The motor has an external fan. The major parameters presented in Table 1.

Table 1. Major parameters of the analyzed motor.

Parameter	Value
stator outer diameter	106 mm
rotor outer diameter	69.6 mm
active axial length	62 mm
air gap length	0.3 mm
number of stator slots	36
number of rotor bars	33
rotor skew	1—slot scale
material of bar	aluminum

The motor and its original rotor are presented in Figures 1 and 2, respectively.

Figure 1. Sg71-6B type motor.

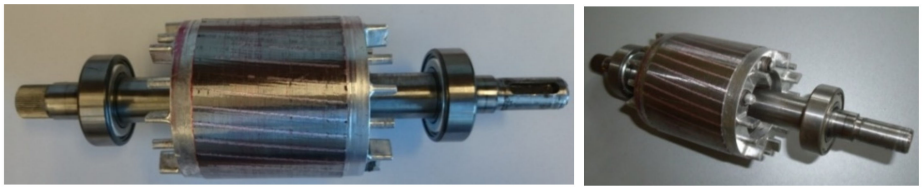

Figure 2. Rotor of the SG71-6B type motor.

In the modified version, the synchronous operation mode was achieved by changing the geometry of the rotor. Six grooves were milled symmetrically, axially, on the circumference of the rotor. The result is a rotor with six clearly formed teeth. In the latter part of this paper, these are interchangeably referred to as large rotor teeth and, by analogy, the resulting notches will be referred to as large rotor grooves. The changes introduced in the rotor area are presented in Figure 3.

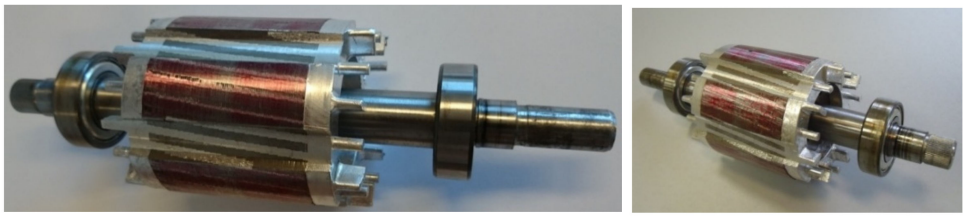

Figure 3. Motor rotor with milled grooves.

In the presented approach, it was assumed that the stator of the motor remains unchanged regarding its structure as well as the winding design.

The torque created in the synchronous motor (1) is the sum of two components synchronous (T_s) and reluctance (T_r). In the modified analyzed structure, the synchronous torque T_s is equal to zero and the reluctance torque T_r created is the result of the difference in reactance in the quadrature q and direct d axes known from the analytical models [6–8,10,11].

$$T = \underbrace{\frac{mUE_f}{\omega_1 X_d} \sin\beta}_{T_s} + \underbrace{\frac{mU^2}{2\omega_1}\left(\frac{1}{X_q} - \frac{1}{X_d}\right) \sin 2\beta}_{T_r}, \quad (1)$$

where m is the number of phases; U is the value of the supply voltage; E_f is the value of the induced electromotive force; ω_1 is the synchronous angular speed; X_d is the reactance in the direct axis of the machine; X_q is the reactance in the quadrature axis of the machine; and β is the angle of the internal load.

An asymmetry in the rotor magnetic circuit (different conditions of electromagnetic field penetration from the stator to the rotor) determines the resultant value of the motor electromagnetic torque, and more precisely, the values of its components (reluctance and synchronous). In the case considered, both components are very important due to the adopted work regime [7,12,13].

The research conducted was aimed at determining the influence of the shape and dimensions of the large tooth when it comes to ensuring the expected values of the synchronous torque.

In Figure 4, the groove requiring milling in the original rotor is primarily dimensioned. This is in opposition to the dimensioning of the large tooth. The proposed description comes as a result of the adopted technology of the modification of the rotor structure (modification by milling).

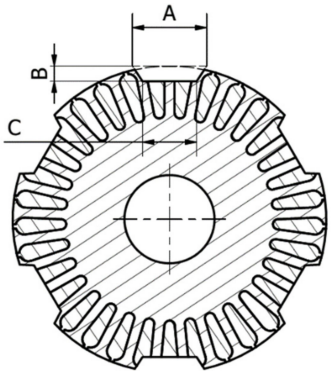

Figure 4. Modified rotor dimensions.

For the results considered, a squirrel-cage induction motor was tested on a specially built test stand, as shown in Figure 5.

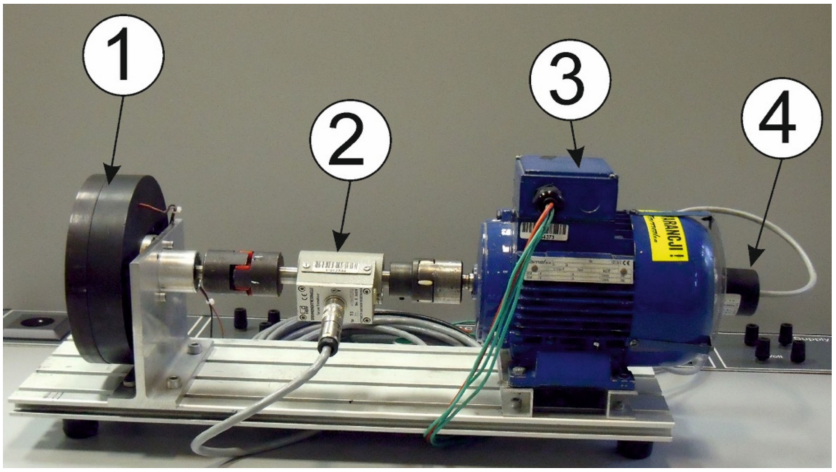

Figure 5. Measuring stand for testing the motors: (1) magnetorheological brake; (2) strain gauge head; (3) tested motor; and (4) encoder.

The major performance characteristics such as winding resistance, idle current as well as efficiency at a rated load of the motor were determined to obtain reference data for further studies as well as to validate the developed numerical models.

Numerical models of the electromagnetic phenomena in the studied induction and reluctance motors were developed. At the preliminary stage of the studies, the planar symmetry of the magnetic field in the motors in question was assumed. Based on the results of the performed 2D finite element analysis, the rotor of the induction motor was modified. The results of this experiment are published in [14]. The studies mentioned allowed us to determine whether further research is advisable and confirmed the correctness of the developed numerical model.

Nevertheless, the assumption of the planar symmetry of the electromagnetic field leads to the neglection of the spatial shape of the rotor cage, which is important regarding the suppression of the torque sub as well as super harmonics during transient states, especially during the start-up process. Therefore, in the presented paper, a numerical, three-dimensional field model was developed and applied. The model, referred to in the literature as the 2 and 1/2 (2D1/2) model, was intentionally abandoned [15–17], despite its high computational complexity. It was found that only the 3D model would fully allow the verification of the correctness of the numerical reproduction of the tested engine. The aim was to make this model accurate enough so that there would be no need to make a physical prototype to evaluate the correctness of new solutions. The developed model takes into account the skew of the cage rotor bars and the geometric structure of the end rings closing

them, the different lengths of the stator and rotor packages as well as the properties of the construction materials used.

3. Numerical Model of the Line-Start Reluctance Motor

The parametric numerical model of the motor was developed by using professional, computer aided design environments created in AutoCAD, Inventor, and COMSOL, and is a three-dimensional model. In the author's model, the geometric structure of the electromagnetic circuit of the motor has been fully reproduced, taking into account the bevel of the squirrel-cage rotor rods, the end rings, and the different lengths of the stator and rotor packages. The parameters of the stator winding were modeled according to the data of the base induction motor (Figure 6).

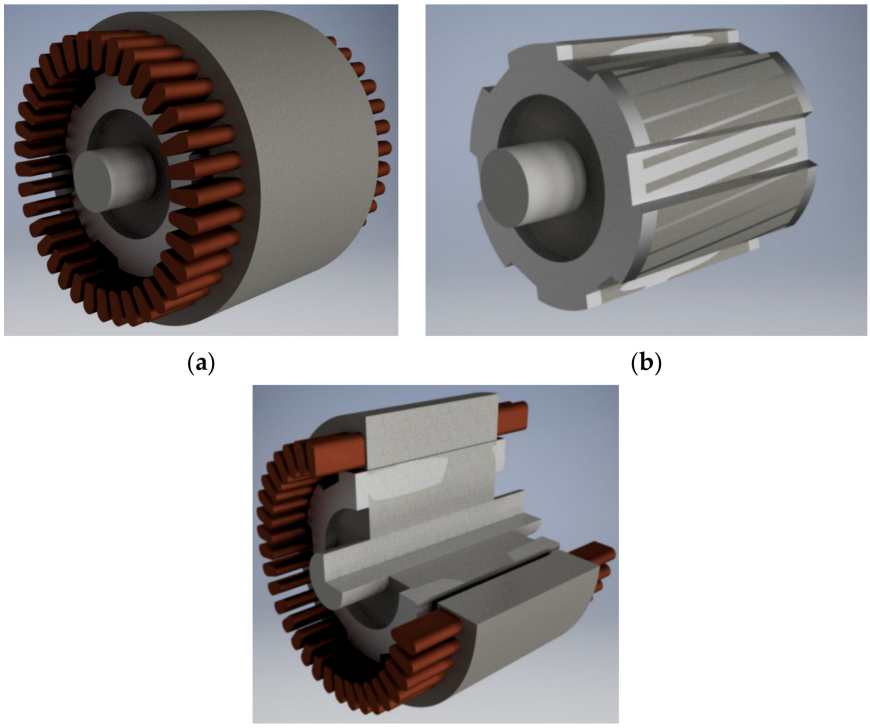

(**a**) (**b**)

(**c**)

Figure 6. CAD model of reluctance motor; (**a**) stator-rotor set; (**b**) rotor; (**c**) partial view—partial cross-section of motor structure without housing and bearing discs.

In the developed CAD model, the AK-1 type aluminum die-cast bearing discs as well as the motor housing were intentionally omitted. These elements do not affect the studied electromagnetic phenomena in the considered machines. A complete digital model of the motor would be needed to test its susceptibility to vibrations, the course of thermal processes, and the distribution of mechanical stress. These phenomena are the subject of separate research. Consideration of all the structural components of the motor would result in a significant increase in calculation time that is not justified at this stage. The shape of the rotor end rings was simplified to reduce the computational complexity of the numerical model of the electromagnetic phenomena. In the real motor, the end rings shown in Figures 2 and 3 serve as "blades" for the internal ventilation fan and brackets for the possible seating of the rotor balancing mass (balancing by adding mass). However, these elements do not take part in the creation of torque, radial forces, or active losses in the conductive part of the rotor and thus can be neglected in the numerical field model of the electromagnetic phenomena. In the numerical model, their introduction would increase the number of finite elements of the mesh, and this would significantly affect the calculation time. However, the role of these elements in the process of air circulation inside

the machine cannot be overlooked. Together with the external fan and bearing units, they are the source of mechanical losses and should be taken into account in the analysis of the start-up process. In the proposed approach, the impact of the bearing and ventilation losses were taken into account by increasing the additional passive mechanical torque load so that it changes as a function of the rotor speed.

After imposing the above discussed simplifications, the developed, three-dimensional FEM model contained over 33,000 nodes and 178,000 tetrahedral elements. It reproduced all components of the motor structure relevant for the electromagnetic calculations. As mentioned, the non-linearity of the magnetic circuit of the motor was taken into account. The magnetization B-H characteristics of the electrical steel sheets provided by the manufacturer were assumed. As the modified structure of the rotor consists of regions that will possibly be saturated, the adoption of non-linear magnetization characteristics for the performed numerical calculations is particularly important in terms of obtaining reliable results, especially in the analysis of the operation of the motor in transient states (e.g., starting). The field model equations were supplemented by circuit equations of the stator windings. The calculations were carried out for stator windings connected in a star arrangement and supplied by a three phase balanced sinusoidal voltage source. In the circuit equations of the model, the inductances of the end connections of the stator windings were taken into account.

Because the magnetic properties of the electrical steel sheets from which the magnetic circuit is made vary significantly during the manufacturing process (punching, pressing, lamination, etc.) [18], it is necessary to "scale" the course of the magnetization characteristics of the real magnetic circuit of the engine. Only such "recalibrated" characteristics can be used in the further calculations of the machine.

For this purpose, first, a number of tests were carried out on the performance parameters of a brand new base/reference asynchronous motor and then the numerical calculations were performed for the corrected magnetization characteristics. The results of both tests were compared. It was assumed that the numerical model was properly calibrated when the discrepancies between the values of torque, current, slip, and time of reaching a steady speed for a given load did not differ by more than 7–10% between both tests. Such a procedure allows to digitally prototype structures with a modified geometry of the rotor while maintaining the original design of the magnetic circuit of the stator and its windings.

In FEM numerical calculations of magnetic circuits, the Coulomb and the Maxwell stress tensor methods are the most frequently used approaches to determine the electromagnetic torque value [6,12,15,19,20]. A high accuracy of results can also be obtained using the method proposed by Arkkio, based on the Maxwell stress tensor method [11,21,22]. In the numerical model developed, the value of the electromagnetic torque was determined by modifying the method [11] for the purpose of calculations in a three-dimensional system (3D). The authors adopted the following formula to determine the value of the electromagnetic torque developed by the motor:

$$T = \frac{1}{\mu_0 \delta} \int_V r B_r B_t \mathrm{d}v, \tag{2}$$

where δ is the value of the air gap; μ_0 is the magnetic permeability of the vacuum; r is the integration radius; B_r, B_t are the values of the radial and tangential components of the magnetic flux density vector, respectively; and V is the volume of the air gap in the active space of the machine.

In the developed model, the rotational movement of the rotor was taken into account by introducing an equation of system dynamics.

As mentioned in the introduction, the numerical model developed introduces the parameterization of the major dimensions of the considered magnetic circuit. The application of parameterization enables the carrying out of variant numerical tests by means of

digital prototyping. The main purpose of the presented calculations was to determine the influence of the shape and dimensions of additional large rotor teeth on the ability of the machine to work at a synchronous rotational speed. The model also makes it possible to study the impact of the following factors:

- phase of the supply voltage at the moment of switching on;
- initial angular position of the rotor against the stator for the start-up process course; and
- values of the moment of inertia and the load torque with user-defined characteristics.

4. Machine Prototype Testing

4.1. Simulation Tests

The numerical model was implemented in the COMSOL environment. In the initial model of the rotor, it was assumed that:

- The main dimensions of the rotor (length, diameter) remained the same as in the induction motor;
- The geometrical structure of the rotor cage (shape and dimensions of the cage bars, shape and dimensions of the cage end rings) was kept the same as in the induction motor; and
- Six symmetrically arranged grooves with dimensions A, B, and C from Figure 4 were cut out of the rotor magnetic circuit, whereas A = 16 mm, B = 4 mm, and C = 12 mm, respectively.

A digital model of such a rotor is shown in Figure 7.

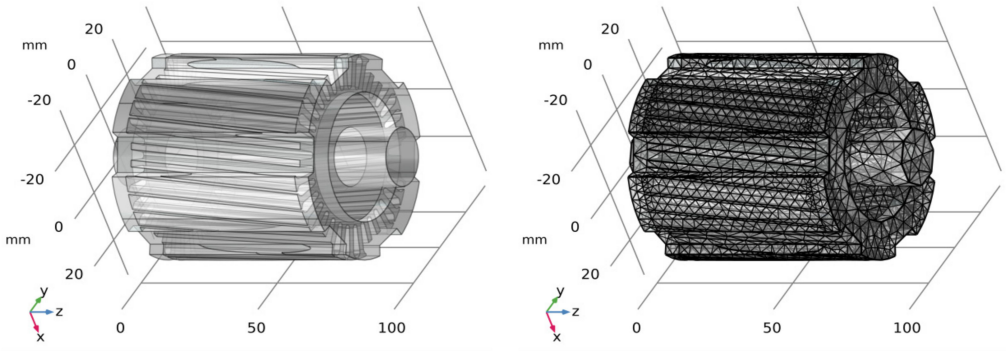

(**a**) (**b**)

Figure 7. Geometry of the rotor: (**a**) structure of the magnetic circuit, (**b**) finite element mesh.

A symmetrical three-phase power supply system described by the following equations was adopted:

$$\begin{aligned} u_A(t) &= \frac{U}{\sqrt{2}}\sin(\omega t + \varphi_0), \\ u_B(t) &= \frac{U}{\sqrt{2}}\sin\left(\omega t - \tfrac{2}{3}\pi + \varphi_0\right), \\ u_C(t) &= \frac{U}{\sqrt{2}}\sin\left(\omega t + \tfrac{2}{3}\pi + \varphi_0\right), \end{aligned} \tag{3}$$

where U is the phase voltage; ωt is the frequency of the supply voltage; and φ_0 is the angle of the phase shift.

The calculations were made for the following conditions:

- Supply voltage U = 400 V, 50 Hz, φ_0 = 0, windings connected in a star; and
- Initial load torque 0.5 Nm. After a time of 0.08 s, the torque increased linearly in accordance with that of Figure 8 (thus, the aerodynamic resistance of the ventilator fan and rotating parts as well as the friction in the bearings were mapped). The initial torque value was chosen on the basis of measurements made for the real object.

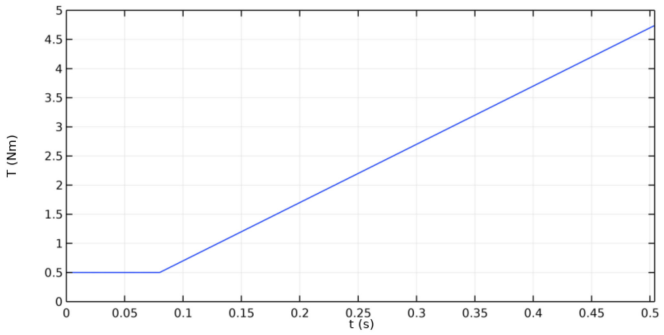

Figure 8. Waveform of the load torque of the motor as a function of time.

The changes in the load torque over time are described by the analytical formula:

$$T(t) = \begin{cases} 0 & 0 \leq t < 0.08 \\ 10(t - 0.08) & t \leq 0.08 \end{cases} \quad [\text{Nm}] \tag{4}$$

The angular position of the rotor in relation to the stator at the moment $t = 0$ s is shown in Figure 9.

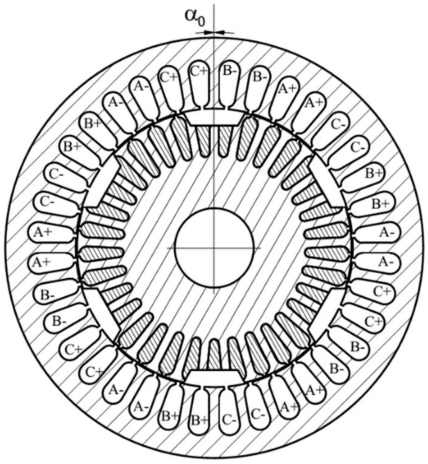

Figure 9. Angular position of the rotor in relation to the stator for $t = 0$ s ($\alpha_0 = 0$).

Figure 10a–c shows the waveforms of the electromagnetic torque developed by the modeled machine (a), rotational speed (b), and currents in stator windings (c) as a function of time:

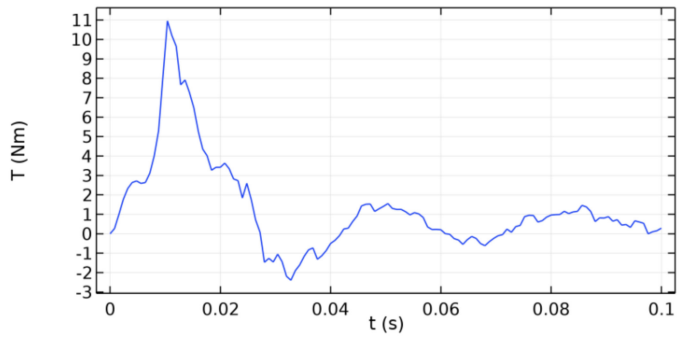

(**a**)

Figure 10. *Cont.*

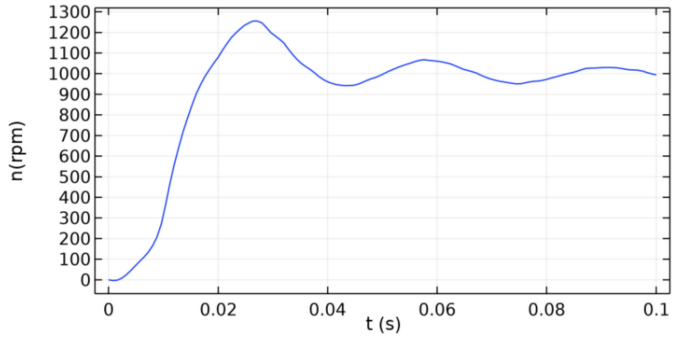

(**b**)

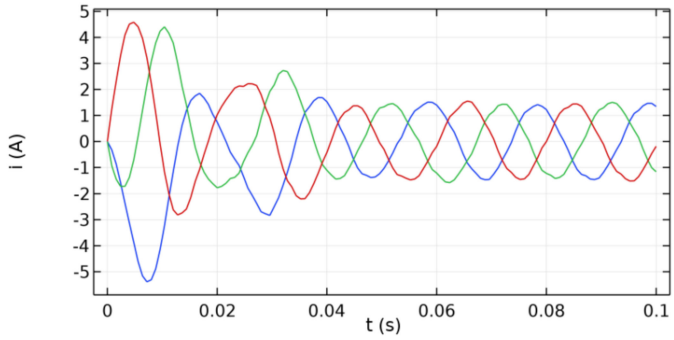

(**c**)

Figure 10. Calculation results: (**a**) electromagnetic torque waveform, (**b**) rotational speed waveform, and (**c**) waveforms of currents in stator windings, the currents of individual phases are marked with green, red, and blue.

The model developed makes it possible to observe the density of currents flowing in the rotor bars and end rings at selected moments in time (Figure 11).

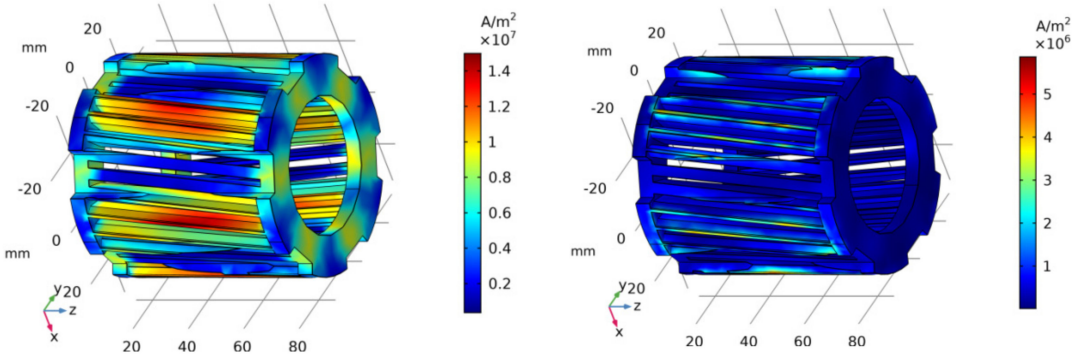

(**a**) (**b**)

Figure 11. Distribution of current density in the rotor winding of the modified motor at different moments time in (**a**) t = 0.0104 s, (**b**) t = 0.1 s.

The calculations showed that the removal of bar fragments did not result in a significant increase in the values of the currents flowing in them.

The adopted structural modifications ensured the possibility of synchronous operation with a load torque exceeding 50% of the rated torque.

For comparison, Figure 12 shows the distributions of current densities in the rotor rods for the following cases: (a) when the rotor rotates synchronously, and (b) when a classic squirrel-cage rotor rotates with a slip of 4%. In both cases, the external loading torque was the same in its value and character.

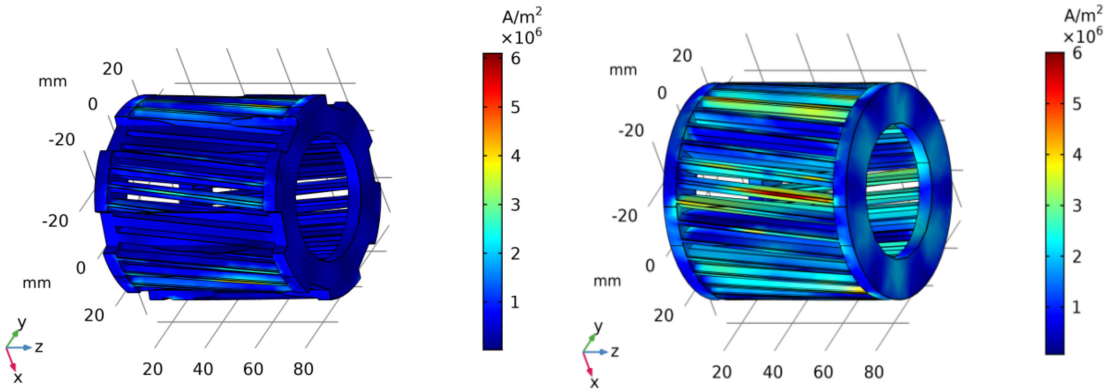

Figure 12. Distribution of current density in the winding of a rotor rotating: (**a**) synchronously; condition reached after 0.082 s from switching on the voltage, (**b**) asynchronously with a slip of 4%; condition reached after 0.053 s.

The developed numerical model allows for relatively simple calculations for practically every rotor structure including those with a changed geometry. For comparison, Figure 13a–c shows the courses of (a) electromagnetic torque, (b) rotational speed, and (c) currents in stator windings, developed by the referenced induction motor as a function of time:

4.2. Physical Model Tests

In accordance with the dimensions adopted in the simulation model, the rotor of the induction motor was modified. Tests of the modified motor were carried out on the test stand showed in Figure 5.

The load torque values were changed during the tests by means of a magnetorheological brake developed and built by the team working with the authors of this paper. The design of that brake allows for the application of a constant value of torque independent of the rotational speed, even when that rotational speed is zero. The torque was measured with a T5 type strain gauge head from Hottinger Baldwin Messtechnik GmbH. The rotational speed was measured by means of an encoder with a resolution of 1024 pulses, coupled to the motor shaft. The output signal from the encoder was recorded with an Agilent DSOX 3034A type digital oscilloscope. A proprietary program that allows for the observation of high precision changes in rotor rotational speed in transition and steady states was specifically developed for the purpose of the measurement tests. A proprietary algorithm analyzing the time course of the impulse encoder signal was implemented in the program. The result of the operation of the algorithm is the determination of momentary rotational speed values as well as a precise determination of the machine rotor's angular position. The results of the calculations are presented in a graphic form or exported to a file.

The results of the tests are shown in Figures 14 and 15.

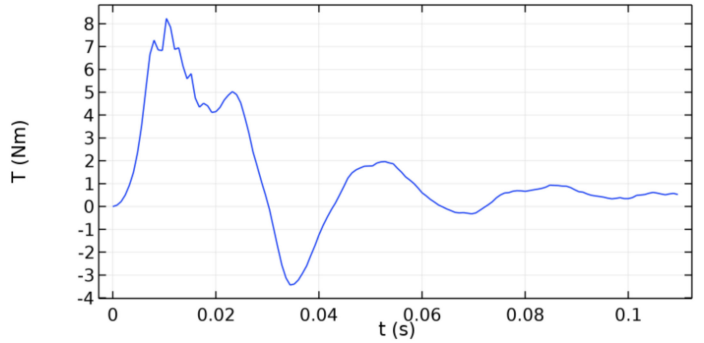

(**a**)

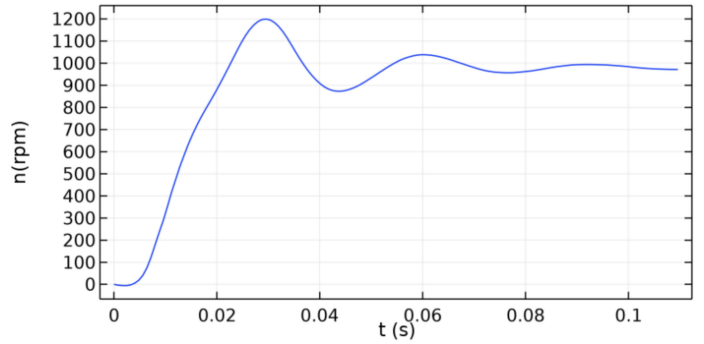

(**b**)

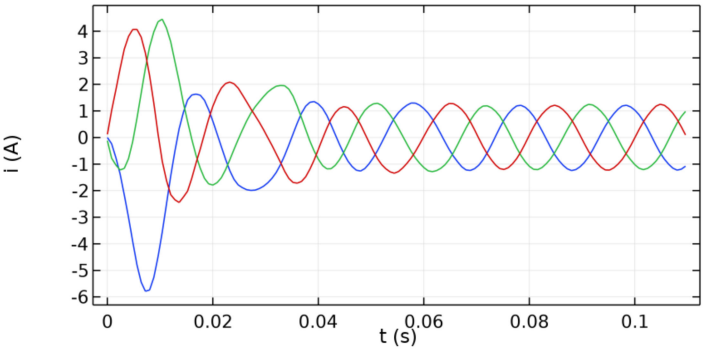

(**c**)

Figure 13. Waveforms of (**a**) electromagnetic torque, (**b**) rotational speed, and (**c**) currents in stator windings, developed by the referenced induction motor as a function of time; the currents of individual phases are marked with green, red and blue.

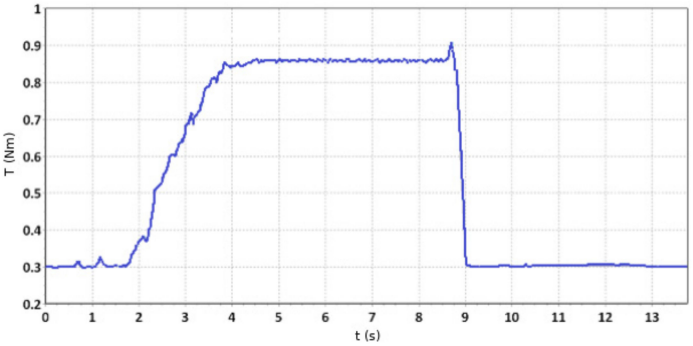

Figure 14. Results of the reluctance motor torque measurement–start-up with load torque increasing to the nominal load of the base induction motor.

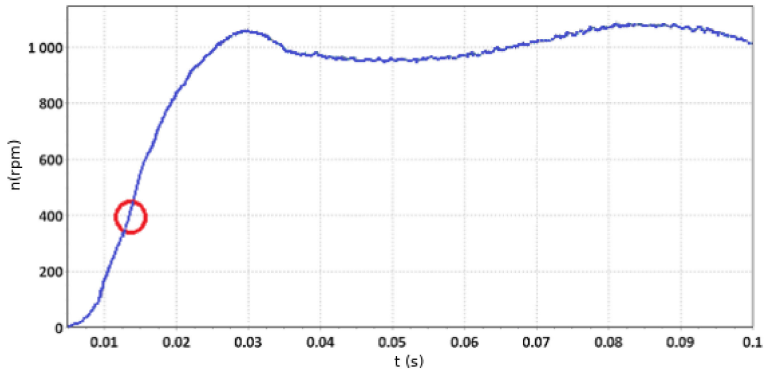

Figure 15. Results of the reluctance motor rotational speed measurement during start-up–the course after processing the measurement results.

Figure 14 shows the start-up of a motor loaded with a torque with a value changing with time. This corresponds to the starting of the motor that drives the fan. Characteristics of the load as a function of time have an exponential course. It was chosen to correspond to the case of the so-called heavy starting (long starting time).

Figure 15 shows changes in the rotational speed of an engine loaded with a constant torque. The instantaneous speed values were determined using the signal from the encoder.

The observed "collapse" of the velocity curve (for the time of approx. 0.015 s, see red circle) results from the uneven air gap (half-open slots of the rotor and stator). This phenomenon applies to both tested models. This effect is noticed by other researchers [23,24].

The physical experiment carried out confirmed the correctness of the adopted concept of the reluctance motor.

5. Reluctance Motor Start-Up Test for Various Initial Conditions

Comparing the results of the physical model tests with the results of the simulation calculations, it was considered that the convergence achieved allows for the thesis that the developed numerical model can be used for further simulation tests.

Many modern drive systems with a reluctance motor require the angular positioning of the rotor shaft or the use of sensors determining the angular position of the rotor shaft in relation to the stator at start-up. Often, the motor supply system has to also provide an appropriate value for the initial phase shift of the supply voltages. The developed structure is a motor that has the ability to self-start without the need for additional systems.

The simulation test results presented below determine the effect of φ_0 angle values (Equation (3)) on the transition state course during start-up—see Figures 16 and 17. The value of the load torque was assumed according to the characteristics from Figure 8.

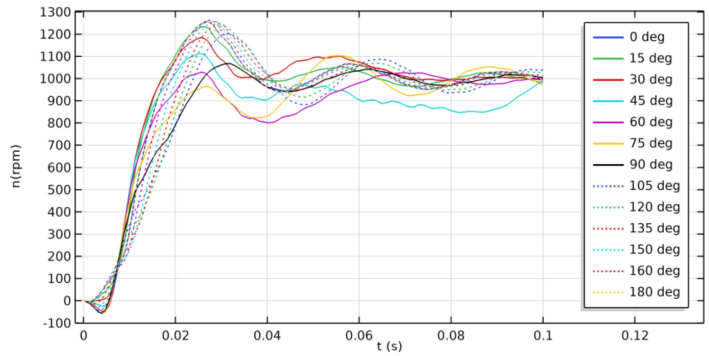

Figure 16. Rotational speed waveforms as a function of time during the start-up of the motor for various φ_0 angle values.

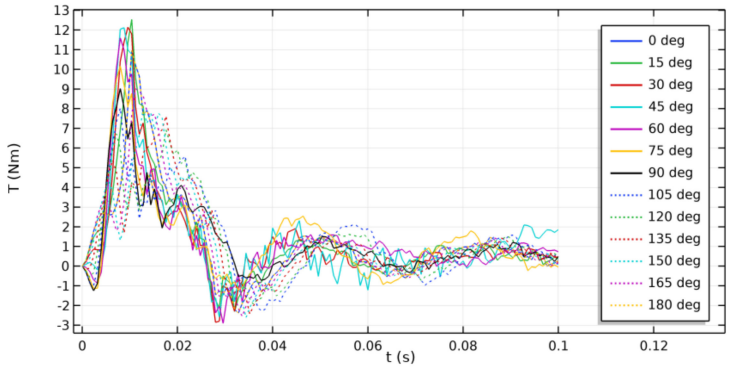

Figure 17. Electromagnetic torque during start-up of the motor for various φ_0 angle values.

The maximum instantaneous starting torque values for various φ_0 angle values are listed in Table 2.

Table 2. The maximum instantaneous starting torque values.

φ_0 (deg)	t(s)	T_{max}(Nm)	$T_{max}/T_{max(\varphi_0)}$(%)
0	0.0104	10.959	100
15	0.0104	12.534	114
30	0.0096	12.139	111
45	0.0088	12.114	111
60	0.008	11.597	106
75	0.008	10.159	93
90	0.008	9.0277	82
105	0.008	8.0266	73
120	0.0176	6.9265	63
135	0.0176	7.6258	70
150	0.016	7.7794	71
165	0.112	9.0112	82
180	0.0104	10.959	100

The experiment has shown that the phase of the supply voltage (φ_0 angle) has a relatively small impact on the start-up process of the model. For practically all the cases considered, the motor achieved synchronous rotational speed for the first time after a time equal to approximately 30 ms. This does not mean that the starting phase is completed after the above-mentioned time. The changes in the maximum torque developed by the model were much greater. If the value of the torque determined for phase angle φ_0 = 0 degrees is taken as a reference, its value for angle φ_0 =120 degrees is only 56%. However, at the load torque given, this value is sufficient to make the rotor operate at a synchronous rotational speed.

The developed model was used to determine the effect of the initial rotor shaft position angle (α_0 according to Figure 9) on the starting parameters of the motor. The simulation test results presented below on Figures 18 and 19. As in previous tests, the value of the load torque was in accordance with the characteristics from Figure 8.

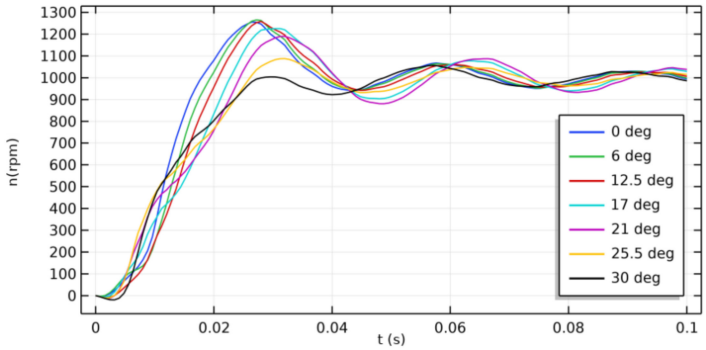

Figure 18. Waveforms of the rotational speed of the motor during start-up for various α_0 angle values.

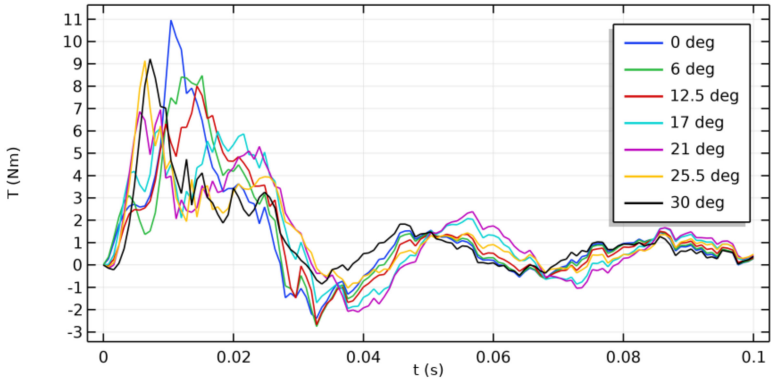

Figure 19. Electromagnetic torque during the start-up of the motor for various α_0 angle values.

The maximum instantaneous starting torque values for various α_0 angle values are listed in Table 3.

Table 3. Starting torque values.

α_0 (deg)	t (s)	T_{max} (Nm)	$T_{max}/T_{max(\alpha 0)}$ (%)
0	0.0104	10.959	100
6	0.0152	8.4802	77
12.5	0.0144	8.0112	73
17	0.0088	6.1125	56
21	0.0088	6.954	63
25,5	0.0064	9.104	83
30	0.0072	9.2226	84

The experiment allows us to claim that the structure in question is capable of synchronous operation regardless of the initial angular position of the rotor in relation to the stator windings. The changes in the value of the maximum electromagnetic torque developed did not exceed 30%.

Therefore, in addition to normal test procedures, the vibrations of the motor body for a motor equipped with both rotor types were measured.

The energy efficiency of the modified motor during synchronous operation with a load torque of 50% of the rated torque of the base induction motor was assessed. In the case under examination, it was 5% more efficient than that of the base motor before its modifications.

A financial analysis of the execution of rotors for completed induction motors was carried out. Taking into account the complex material structure of a completed squirrel cage rotor, the application of the method of milling large grooves in the rotors only after their execution as asynchronous motor rotors was considered. Taking into account the need

of a CNC machine tool, a comparison of several providers of such services was compared and a determination was made that the cost of such an operation, given a batch of rotors not requiring additional mechanical work and not exceeding 100–150 pieces per month, would result in an increase in the price of the motor by about 5–6.5%. Taking into account the changes in the efficiency of the motor, this means that replacing the rotor, despite its higher purchase price, should bring some small financial benefits to the user after a year of motor operation. The proposed design modifications of the motor do not require specialist mechanical work and can be performed both at the motor production stage and as a modernization of a machine already installed in a drive system.

The tests were carried out in accordance with the standards found in the literature [25,26] (i.e., in idle running conditions). An ICP type vibration sensor was mounted in the same place every time. The test results are presented in Table 4.

Table 4. Vibration speed.

Induction Motor (IM)		Reluctance Motor (LSRM)	
Axis	**Vibration Speed (mm/s)**	**Axis**	**Vibration Speed (mm/s)**
X	0.79	*X*	0.78
Y	0.64	*Y*	0.79
Z	1.05	*Z*	1.12

The axes were adopted as follows: *X* axis—directed parallel to the axis of the machine; *Y* axis—directed perpendicularly to the axis of the machine, parallel to the plane defined by the feet of the machine; and *Z* axis—directed perpendicularly to the axis of the machine and to the plane defined by the feet of the machine.

The motor in both versions meets the requirements of the aforementioned standards.

In the case of the LSRM (line start reluctance motor) motor, the vibration speed amplitude was approximately 8% higher than that of the IM motor (induction motor).

6. Conclusions

The measurements confirmed the correctness of the adopted calculation strategy using full three-dimensional numerical models. The calculation time for such models is significant (several dozen hours) due to their complex structure and the need to take into account the following considerations:

- the non-linearity of the magnetic circuit of the stator and rotor;
- voltage forcing;
- the complex three-dimensional structure of the magnetic circuit (skew of the rotor grooves with straight additional straight large teeth); and
- the rotating rotor and parameterization of the model in terms of several factors (initial angular position, phase of the supply voltage, rotor geometry).

A solution to reduce this inconvenience is to perform calculations using a cluster consisting of several interconnected PC class computers.

The application of the 2 and 1/2 D method considered during the preparation of the experiment and also described and recommended in the literature [16,17,21] would not allow for a sufficiently precise representation of the three-dimensional structure of the tested object. The calculation time, however, would be much shorter. The precision of the calculations was assumed to take precedence over the costs related to their execution.

Comparing the courses of the torque developed by the motor with the original rotor (Figure 13a) with the course of the torque developed by the reluctance motor, some slight pulsations of this torque can be observed in the case of structures with additional large teeth. Even though the suppressive character of the moment of inertia of all the moving parts as well as the introduction of a non-zero frictional moment were taken into account in the calculations, this phenomenon, associated with the unevenness of the stator-rotor air gap, was still expected. The presence of variable components during the torque developed

by the motor, however, is not desirable from a user's point of view. Therefore, in addition to normal test procedures, the vibrations of the motor body for a motor equipped with both rotor types have been measured.

Author Contributions: Conceptualization, P.I. and K.K.; Methodology, P.I. and K.K.; Software, P.I. and K.K.; Validation, P.I. and K.K; Formal analysis, P.I. and K.K.; Investigation, P.I. and K.K.; Resources, P.I.; Data curation, P.I.; Writing—original draft preparation, P.I.; Writing—review and editing, P.I. and K.K.; Visualization K.K.; Supervision, P.I. and K.K.; Project administration, P.I. and K.K.; Funding acquisition, P.I. and K.K. All authors have read and agreed to the published version of the manuscript.

Funding: This research was funded by the Polish Government, grant number 0212/SBAD/0514.

Data Availability Statement: Not applicable.

Conflicts of Interest: The authors declare no conflict of interest.

References

1. Buiatti, G.M.; Cruz, S.M.A.; Cardoso, A.J.M. Lifetime of Film Capacitors in Single-Phase Regenerative Induction Motor Drives. In Proceedings of the 2007 IEEE International Symposium on Diagnostics for Electric Machines, Power Electronics and Drives, Cracow, Poland, 6–8 September 2007; pp. 356–362.
2. Hirschmann, D.; Tissen, D.; Schroder, S.; De Doncker, R.W. Reliability Prediction for Inverters in Hybrid Electrical Vehicles. *IEEE Trans. Power Electron.* **2007**, *22*, 2511–2517. [CrossRef]
3. Song, Y.; Wang, B. Survey on Reliability of Power Electronic Systems. *IEEE Trans. Power Electron.* **2013**, *28*, 591–604. [CrossRef]
4. Falck, J.; Felgemacher, C.; Rojko, A.; Liserre, M.; Zacharias, P. Reliability of Power Electronic Systems: An Industry Perspective. *IEEE Ind. Electron. Mag.* **2018**, *12*, 24–35. [CrossRef]
5. Wang, H.; Ma, K.; Blaabjerg, F. Design for Reliability of Power Electronic Systems. In Proceedings of the IECON 2012-38th Annual Conference on IEEE Industrial Electronics Society, Montreal, QC, Canada, 25–28 October 2012; pp. 33–44.
6. Gieras, J.F.; Wing, M. *Permanent Magnet Motor Technology: Design and Applications*; Marcel Dekker: New York, NY, USA, 2002; ISBN 978-0-8247-0739-2.
7. Ozcelik, N.G.; Dogru, U.E.; Imeryuz, M.; Ergene, L.T. Synchronous Reluctance Motor vs. Induction Motor at Low-Power Industrial Applications: Design and Comparison. *Energies* **2019**, *12*, 2190. [CrossRef]
8. Kärkkäinen, H.; Aarniovuori, L.; Niemelä, M.; Pyrhönen, J.; Kolehmainen, J. Technology Comparison of Induction Motor and Synchronous Reluctance Motor. In Proceedings of the IECON 2017-43rd Annual Conference of the IEEE Industrial Electronics Society, Beijing, China, 29 October–1 November 2017; pp. 2207–2212.
9. Niedworok, A.; Orzech, L. Porównanie Sprawności Napędu Wyposażonego w Silnik Indukcyjny i Reluktancyjny. *Prz. Elektrotech.* **2016**, *92*, 246–250. [CrossRef]
10. Boldea, I. *Electric Machines: Steady State, Transients, and Design with MATLAB*; CRC Press: Boca Raton, FL, USA, 2009; ISBN 978-0-429-11223-2.
11. Lipo, T. Synchronous Reluctance Machines-A Viable Alternative for AC Drives? *Electr. Mach. Power Syst.* **1991**, *19*, 659–671. [CrossRef]
12. Chen, Q.; Tang, Y.; Lomonova, E.A. Torque Optimization of Synchronous Reluctance Motor for Electric Powertrain Application. In Proceedings of the 2019 Fourteenth International Conference on Ecological Vehicles and Renewable Energies (EVER), Monte-Carlo, Monaco, 8–10 May 2019; pp. 1–7.
13. Knebl, L.; Bacco, G.; Bianchi, N.; Ondrusek, C. Synchronous Reluctance Motor Analytical Model Cross-Saturation and Magnetization Analysis. *Prz. Elektrotech.* **2020**, *1*, 110–114. [CrossRef]
14. Idziak, P.; Kowalski, K. Impact of Rotor Design on Motion Properties of a Synchronized Induction Motor. In Proceedings of the 2018 14th Selected Issues of Electrical Engineering and Electronics (WZEE), Szczecin, Poland, 19–21 November 2018; pp. 1–4.
15. Hameyer, K.; Mertens, R.; Pahner, U.; Belmans, R. New Technique to Enhance the Accuracy of 2-D/3-D Field Quantities and Forces Obtained by Standard Finite-Element Solutions. *IEE Proc. Sci. Meas. Technol.* **1998**, *145*, 67–75. [CrossRef]
16. Lai, H.C.; Rodger, D. Modelling Rotor Skew in Induction Machines Using 2D and 3D Finite Element Schemes. In Proceedings of the 1997 IEEE International Electric Machines and Drives Conference Record, Milwaukee, WI, USA, 18–21 May 1997; pp. WB3/5.1–WB3/5.3.
17. Dudzikowski, I.; Ciurys, M. *Komutatorowe i Bezszczotkowe Maszyny Elektryczne Wzbudzane Magnesami Trwałymi*; Oficyna Wydawnicza Politechniki Wrocławskiej: Wrocław, Poland, 2011.
18. Sundaria, R.; Lehikoinen, A.; Arkkio, A.; Belahcen, A. Effects of Manufacturing Processes on Core Losses of Electrical Machines. *IEEE Trans. Energy Convers.* **2021**, *36*, 197–206. [CrossRef]
19. Silwal, B.; Rasilo, P.; Perkkiö, L.; Hannukainen, A.; Eirola, T.; Arkkio, A. Evaluation and Comparison of Different Numerical Computation Methods for the Electromagnetic Torque in Electrical Machines. In Proceedings of the 2013 International Conference on Electrical Machines and Systems (ICEMS), Busan, Korea, 26–29 October 2013; pp. 837–842.

20. Tarnhuvud, T.; Reichert, K. Accuracy Problems of Force and Torque Calculation in FE-Systems. *IEEE Trans. Magn.* **1988**, *24*, 443–446. [CrossRef]
21. Arkkio, A.; Hannukainen, A. Proper Finite-Element Discretization for Torque Computation of Cage Induction Motors. In Proceedings of the Automation and Motion International Symposium on Power Electronics Power Electronics, Electrical Drives, Sorrento, Italy, 20–22 June 2012; pp. 1456–1461.
22. Arkkio, A. *Analysis of Induction Motors Based on the Numerical Solution of the Magnetic Field and Circuit Equations*; Helsinki University of Technology: Helsinki, Finland, 1987; p. 59.
23. Castagnini, A.; Känsäkangas, T.; Kolehmainen, J.; Termini, P.S. Analysis of the Starting Transient of a Synchronous Reluctance Motor for Direct-on-Line Applications. In Proceedings of the 2015 IEEE International Electric Machines Drives Conference (IEMDC), Coeur d'Alene, ID, USA, 10–13 May 2015; pp. 121–126.
24. Pietrowski, W.; Górny, K. Analysis of Torque Ripples of an Induction Motor Taking into Account a Inter-Turn Short-Circuit in a Stator Winding. *Energies* **2020**, *13*, 3626. [CrossRef]
25. IEC 60034-14. *Rotating Electrical Machines—Part 14: Mechanical Vibration of Certain Machines with Shaft Heights 56 mm and Higher—Measurement, Evaluation and Limits of Vibration Severity*; ANSI: New York, NY, USA, 2018.
26. ISO 220816-1:2016 Mechanical Vibration-Evaluation of Machine Vibration by Measurement on Non Rotating Parts—Part 1: General Guidelines. Available online: https://www.iso.org/obp/ui/#iso:std:iso:20816:-1:ed-1:v1:en (accessed on 1 April 2021).